Research Article Vol. 4, No. 11 / November 2017 / Optica 1317

Complete coherent control of silicon vacancies in diamond nanopillars containing single defect centers

Jingyuan Linda Zhang,[1,7,†] Konstantinos G. Lagoudakis,[1,6,†] Yan-Kai Tzeng,[4] Constantin Dory,[1] Marina Radulaski,[1] Yousif Kelaita,[1] Kevin A. Fischer,[1] Shuo Sun,[1] Zhi-Xun Shen,[2,3,4] Nicholas A. Melosh,[2,3] Steven Chu,[4,5] and Jelena Vučković[1]

[1]E. L. Ginzton Laboratory, Stanford University, Stanford, California 94305, USA
[2]Geballe Laboratory for Advanced Materials, Stanford University, Stanford, California 94305, USA
[3]Stanford Institute for Materials and Energy Sciences, SLAC National Accelerator Laboratory, Menlo Park, California 94025, USA
[4]Department of Physics, Stanford University, Stanford, California 94305, USA
[5]Department of Molecular and Cellular Physiology, Stanford University, Stanford, California 94305, USA
[6]e-mail: lagous@stanford.edu
[7]e-mail: ljzhang@stanford.edu

Received 5 April 2017; revised 21 September 2017; accepted 22 September 2017 (Doc. ID 291746); published 23 October 2017

Arrays of identical and individually addressable qubits lay the foundation for the creation of scalable quantum hardware such as quantum processors and repeaters. Silicon-vacancy (SiV) centers in diamond offer excellent physical properties such as low inhomogeneous broadening, fast photon emission, and a large Debye–Waller factor. The possibility for all-optical ultrafast manipulation and techniques to extend the spin coherence times makes them promising candidates for qubits. Here, we have developed arrays of nanopillars containing single (SiV) centers with high yield, and we demonstrate ultrafast all-optical complete coherent control of the excited state population of a single SiV center at the optical transition frequency. The high quality of the chemical vapor deposition (CVD) grown SiV centers provides excellent spectral stability, which allows us to coherently manipulate and quasi-resonantly read out the excited state population of individual SiV centers on picosecond timescales using ultrafast optical pulses. This work opens new opportunities to create a scalable on-chip diamond platform for quantum information processing and scalable nanophotonics applications.

OCIS codes: (160.2220) Defect-center materials; (270.0270) Quantum optics; (270.1670) Coherent optical effects.

https://doi.org/10.1364/OPTICA.4.001317

1. INTRODUCTION

Deterministic positioning of individual quantum emitters with nearly identical properties is an outstanding challenge to the creation of large scale quantum hardware. Recent technological leaps have enabled the development of high-quality, site-controlled quantum dots that have attracted strong interest because of their potential use as building blocks in scalable quantum hardware [1–3]. However, the inhomogeneous broadening of such emitters still imposes limitations for large-scale integration. An alternative that has arisen for scalable qubits are the nitrogen vacancy (NV) centers in diamond, due to the excellent spin properties under ambient conditions [4–6] and the potential for on-demand positioning [7,8]. However, spectral diffusion and the large phonon sideband limit both the quality of coherent photon generation from NV centers and their ability to be integrated in devices that might have nearby free surfaces.

Most recently, Silicon-vacancy (SiV) centers in diamond have attracted attention as a potential candidate for qubits. Due to the inversion symmetry of the color center [9], SiVs offer spectral stability [10], strong emission into the zero phonon line [11], and narrow inhomogeneous broadening [9,12]. Remarkable efforts have been made to yield nanophotonic devices in bulk diamond, for integration of these color centers into a photonic network [13–19], and to deterministically position them [20]. In the meantime, the spin coherence time has been measured [21,22], and techniques to coherently control the SiV optical transition [23,24], orbital ground states [24], and electronic spin states [25] are under active investigation. Moreover, complete SU(2) control of the state of a SiV center, which involves rotation of the Bloch vector around an arbitrary axis on the Bloch sphere, is a critical function to achieve in quantum information processing. However, ultrafast coherent control of low strain SiV centers in a nanophotonic structure using any method remains elusive. In our work, we combine the nanotechnology that produces high-quality SiV centers in nanopillars and ultrafast all-optical coherent control to demonstrate complete SU(2) quantum control of the optical transition of single SiV centers in nanostructures containing individual SiV centers for what we believe is the first time. The ability to coherently control SiV centers in nanostructures is a prerequisite for their application in quantum photonic

devices. The possibility to perform complete SU(2) control over the optical transition also lays the ground work for schemes that take advantage of geometric phases to coherently control the orbital ground states [26].

Here we fabricated regular arrays of diamond nanopillars containing individual SiV centers with high yield and spectral stability, using diamond grown by chemical vapor deposition (CVD) followed by electron-beam lithography and dry etching to generate the nanophotonic structures. Taking advantage of the exceptional properties of SiV centers in diamond, we use this promising platform to demonstrate complete SU(2) coherent control of the optical transition of single SiV centers in nanopillars using ultrafast optical pulses, enabled by the high post-fabrication spectral stability of the SiV centers. The ability to coherently control an isolated low strain SiV center on a picosecond timescale, in a nanostructure tens of nanometers from the diamond surface, paves the way toward scalable on-chip integration of these diamond-defect centers into nanophotonic devices for highly scalable quantum hardware.

2. MATERIALS AND METHODS

The sample is grown by the microwave plasma chemical vapor deposition (MPCVD) method on a high purity type IIa diamond substrate from Element Six. Nominally, a 100-nm-thick layer of diamond containing SiV is grown homoepitaxially on the diamond substrate, with the following growth conditions: H_2:300 sccm; CH_4:0.5 sccm; stage temperature 650°C; microwave power 1.3 kW; and pressure: 23 Torr. The silicon atoms are generated from the hydrogen plasma etching of the silicon wafer (8 mm by 6 mm) that is placed under the diamond substrate, and SiV centers are subsequently formed through silicon incorporated into the grown layer by plasma diffusion. Following growth, a pattern of 8 by 8 arrays of diamond nanopillars with interleaved crossbars is exposed in a hydrogen silsesquioxane (HSQ) mask using electron-beam lithography (the crossbars are added as markers to facilitate locating the nanopillars under white light imaging). Finally, an oxygen-based reactive ion etching (RIE) transfers the pattern into the diamond, and the HSQ mask is removed in hydrofluoric acid, resulting in bare diamond pillars. The bare nanopillars are 135–170 nm in diameter and 200 nm in height, and the design choices of the doped layer thickness, pillar height, and pillar diameter were based on the SiV density to produce ∼1 SiV per pillar. Scanning electron microscope (SEM) images of a nanopillar array and a single nanopillar are shown in Figs. 1(a) and 1(b), respectively. In addition to the arrays, we have incorporated large square areas on the same sample to produce a minimally strained environment that yields an ensemble of SiV centers comparable to those in bulk diamond.

The photoluminescence (PL) spectrum at 10 K of the single SiV in the nanopillar under investigation is presented in Fig. 1(c) (red), superposed with the PL from an ensemble of SiVs in bulk diamond (black). The SiV centers in the nanopillars show low spectral shifting compared to those in the low-strain bulk diamond, with the energy of each transition lying within the inhomogeneous distribution of the SiV ensemble in bulk. The height of the nanopillars is greater than the thickness of the epilayer containing the SiVs, such that after the etching, the SiV centers are confined in the nanostructures masked by the negative tone resist. This is confirmed by scanning confocal microscopy of the sample surface, as shown in Fig. 1(d). The custom-made

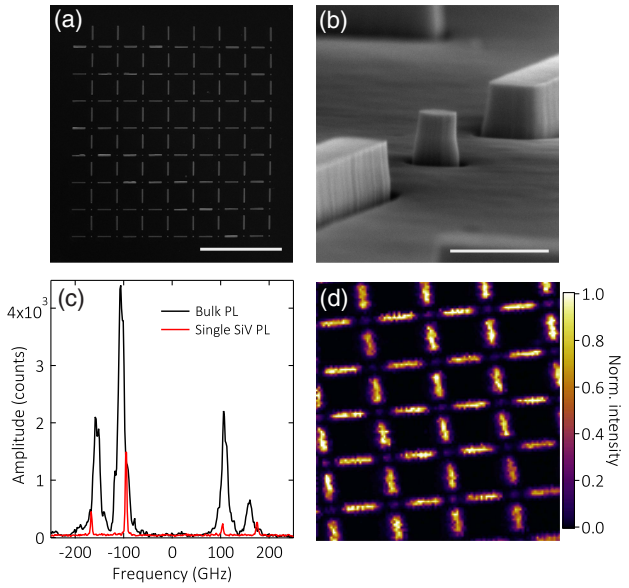

Fig. 1. (a) Scanning electron microscopy (SEM) image of a nanopillar array. Scale bar, 10 μm. (b) SEM image of a 165 nm diameter, 200 nm tall nanopillar. Scale bar, 400 nm. (c) Photoluminescence spectrum from a single nanopillar (red) compared with that from a SiV ensemble in bulk diamond (black). (d) Scanning confocal microscopy map of a representative portion of a nanopillar array on a higher SiV center density sample. The bright areas with higher photon count rate correspond to the areas containing SiV centers, while the background is SiV center free. The count rates observed in the nanopillars are ∼500–1000 cps.

laser scanning confocal microscope consists of a 532 nm CW laser focused onto the sample surface through a high numerical aperture (NA = 0.75) microscope objective, while the photoluminescence (PL) from the excited spot is collected through the same objective, filtered by a dichroic and a long pass filter, into a single mode fiber. The excitation/collection spot is scanned across the sample surface with a fast steering mirror. The PL signal is sent either to a single photon counting module (SPCM) for construction of the PL map [Fig. 1(d)] or to a high-resolution spectrometer for spectroscopic analysis [Fig. 1(c)]. In the PL map of a representative portion of a nanopillar array on a higher SiV density sample in Fig. 1(d), the crossbars and nanopillars containing SiV centers produce high photon count rates under 532 nm laser excitation, and the photoluminescence (PL) spectra from these areas confirm the presence of SiV centers while the spectra from the background areas show no SiV emission (not shown).

The fabricated nanopillar arrays contain isolated single SiV centers with high yield. A statistical study of the PL spectra was conducted on several arrays, one of which is presented in Supplement 1. In the case of more than one emitter per nanopillar, due to the inhomogeneous distribution and in some cases the presence of strain, the spectra contain distinguishable sets of four transitions associated with each SiV center. Therefore, by counting the number of narrow lines in each PL spectrum, one can estimate the number of color centers in each nanopillar. Out of the 64 nanopillars investigated within an entire array, 40, 20, and 4 nanopillars contain 0, 1, and 2 SiV centers per pillar, respectively, consistent with a Poisson distribution with an average value of 0.44. Second-order autocorrelation measurements of $g^{(2)}(\tau)$ yield $g^{(2)}(0) = 0.29$ (see Supplement 1), limited by the

timing jitter of the detector, corroborating the single emitter nature of the SiV in nanopillar structures, and further supporting the conclusions from the spectroscopic study. Based on the statistics of the number of SiV centers embedded in the pillars, we deduce the density of SiV centers in the epilayer to be $\sim 3 \times 10^{14}$ cm^{-3}.

The spectroscopic studies were performed using an above-band excitation laser at 720 nm in combination with a custom-built double grating spectrometer with ~5.0 GHz resolution. Coherent control of the SiV center was performed with spectrally filtered resonant pulses from a mode-locked Ti:Sapphire laser, which allows for addressing individual transitions. The double-grating spectrometer enables the spectral filtering of the emission from individual transitions, which is subsequently collected by a single photon counting module (SPCM) while rejecting light from the resonant spectrally filtered pulses.

3. EXPERIMENTS

Having identified the pillars with individual SiV centers, we then proceed with the demonstration of all-optical coherent manipulation. At a low temperature (10 K), the PL spectrum of the SiV center under investigation displays four narrow peaks [Fig. 2(a)], corresponding to the four radiative transitions between the two excited states and the two ground states, as shown in the inset of Fig. 2(a). To manipulate the state of the SiV center, a linearly polarized, spectrally filtered picosecond optical pulse is applied to resonantly drive the transition $|4\rangle \leftrightarrow |2\rangle$. The spectral shape of the resonant driving pulse is shown as the blue shaded area in Fig. 2(a). Assuming a Gaussian pulse shape, the time-bandwidth product limited pulse duration is 9.1 ps. The pulse coherently rotates the state between the upper ground state $|2\rangle$ and the upper excited state $|4\rangle$, where we define these two levels as our qubit. Because of fast phonon-mediated relaxation processes between the two excited states, as shown by the grey arrow in the inset of Fig. 2(a), level $|3\rangle$ is populated proportionally to the population of level $|4\rangle$. A modulation of the upper excited state population thereby modulates the fluorescence intensity of transition $|3\rangle \rightarrow |1\rangle$. Using the double spectrometer, we spectrally filter the transition $|3\rangle \rightarrow |1\rangle$, which is used as the detection channel [yellow shaded area in Fig. 2(a)]. Detection of a photon from this transition indicates that the system has been set to state $|1\rangle$. Due to the short orbital relaxation time of the ground states of the SiV, level $|2\rangle$ is thermally repopulated according to the Boltzmann distribution [27] and a new qubit rotation between $|4\rangle \leftrightarrow |2\rangle$ may occur. Because the transition $|3\rangle \rightarrow |1\rangle$ is ~200 GHz away from our resonant pulses, this detection scheme enables us to take full advantage of the double spectrometer and almost entirely suppress leakage of the pulses in our detection channel. Moreover, to the best of our knowledge, this is the first demonstration of coherent control of individual SiV centers in diamond through direct detection of the SiV zero phonon line emission. Previous studies of the dynamics of the SiV center have been performed by collecting the phonon sideband [21,22,24].

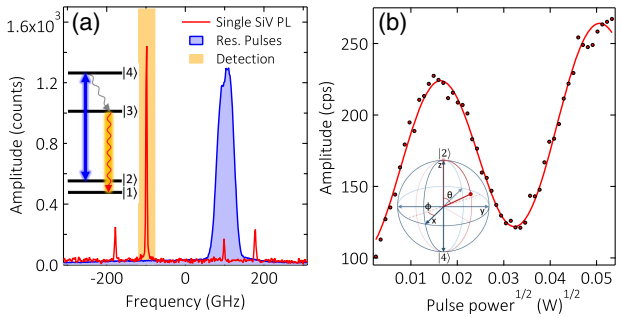

Fig. 2. (a) Excitation and detection scheme of the coherent control experiment. Transition $|2\rangle \leftrightarrow |4\rangle$ of the single SiV center (our qubit) is resonantly addressed with a pulsed Ti:Sapphire laser (blue shaded line), while the radiative emission from transition $|3\rangle \rightarrow |1\rangle$ is detected through a double monochromator by an SPCM (yellow shaded area). Inset shows the energy levels of the SiV center. The double-sided thick blue arrow denotes the coherent interaction of the SiV with the resonant pulses and the red wavy downward arrow denotes the detected photons coming from transition $|3\rangle \rightarrow |1\rangle$. (b) Demonstration of Rabi rotations. Varying the area of the resonant pulses rotates the qubit around the x-axis with a direct impact on the detected photon counts from transition $|3\rangle \rightarrow |1\rangle$, which shows clear oscillations in detected photon counts as a function of the pulse area. The fit function used is $f(p) = a + b \cdot \sin(c \cdot p + d) + e \cdot p^2$, with $\{a, b, c, d, e\} = \{161.05, 58.239, 186.71, -1.4371, 17804\}$. These terms were not independently measured.

The effect of the resonant pulses on the upper excited state population is shown in Fig. 2(b). The pulses induce Rabi rotations on our qubit that are evidenced by oscillations of the detected photon counts as a function of the pulse area. The measured rotation angle extends to 3π, as shown in Fig. 2(b), with the solid red curve representing a sinusoidal fit with a linear background proportional to the power due to leakage of the resonant pulses into the detection channel. On the Bloch sphere [inset of Fig. 2(b)], this corresponds to a rotation of the Bloch vector around the x-axis, bringing the qubit from the north (state $|2\rangle$) to the south pole (state $|4\rangle$) and back.

To demonstrate the rotation of the qubit around an arbitrary axis on the Bloch Sphere, we proceeded with the demonstration of Ramsey interference. A Ramsey interference experiment requires two $\pi/2$ pulses and a variable interpulse delay τ—the first pulse introduces a $\theta = \pi/2$ Rabi rotation of the Bloch vector around the x-axis, and the second pulse further rotates the Bloch vector by $\theta = \pi/2$ around an axis that is at $\varphi = \omega_L \tau$ from the x-axis, with τ the delay between the two pulses and ω_L the frequency of the driven transition. For $\varphi = 2n\pi$, the second pulse brings the Bloch vector to state $|4\rangle$, resulting in maximum counts, whereas for $\varphi = (2n + 1)\pi$ the Bloch vector is brought back to state $|2\rangle$ and the resulting detected counts are at a minimum. A continuous variation of the interpulse delay results in a "figure eight" path on the Bloch sphere, with the two tips located at the north and south poles of the sphere and the central cross point along the y-axis on the equator. To avoid interference between the two $\pi/2$ pulses, we tune the coarse interpulse delay to $\tau \geq 66.7$ ps, implemented using a Michelson interferometer with a motorized delay stage in one arm for the coarse delay and a piezoelectric actuator in the other arm for the fine delay. Ramsey interference is obtained with the piezoelectric actuator, which introduces fine delays on the order of 10 fs, which is enough to resolve the oscillations at the optical frequency. An example of the Ramsey interference at a coarse delay of 100.08 ps is shown in the inset of Fig. 3(a). The oscillations are fitted with a sinusoidal function, from which we extract the contrast of the oscillations for the particular coarse delay. It is important to note that a Ramsey experiment is a quantum interference phenomenon, and therefore it is sensitive to both the frequency stability of the emitter and the phase stability

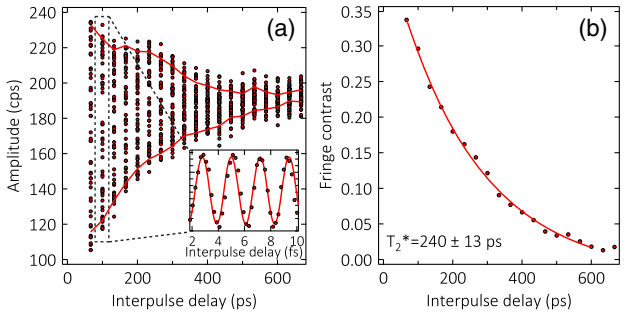

Fig. 3. (a) Ramsey interference for coarse interpulse delays ranging from 66.7 to 667.2 ps. At each coarse delay, we record the Ramsey interference by varying the fine delay over 10 fs, and then fit it with a sinusoidal function as shown in the inset. Fitted amplitude of the Ramsey interference at each coarse delay is shown by the red envelope. (b) Decay of the Ramsey fringe contrast extracted from the data in (a) (red filled circles). The contrast decay is fitted with a single exponential decay function that yields a decay time T_2^* of 240 ps for the qubit.

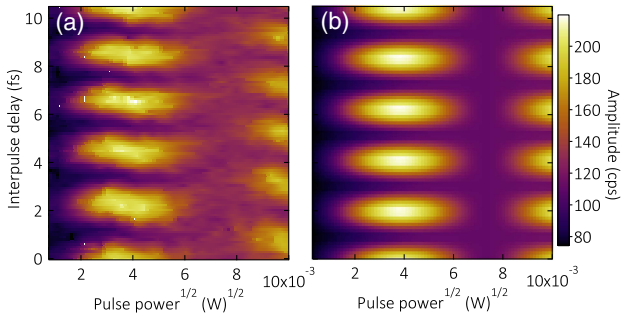

Fig. 4. Experimental (a) and simulated (b) SU(2) control of the upper excited state population. Detected counts for dual pulse excitation with variable pulse area and delay. Here, the angle of rotation per pulse on the Bloch sphere is varied with the pulse area, while the axis around which the state is rotated is controlled with the delay between pulses. The data was taken for a coarse interpulse delay of 66.7 ps.

of the set-up—an interpulse delay fluctuation or emitter frequency shift manifests itself as a phase shift in the Ramsey interference. Therefore, the high-quality Ramsey interference in the inset of Fig. 3(a) shows the exceptional stability of our quantum emitters and the experimental apparatus. Repeating this experiment for a series of coarse delays [Fig. 3(a), red filled circles] allows us to estimate the dephasing time T_2^* of the qubit. In particular, by fitting a single exponential decay function [25] to the Ramsey interference contrast decay in Fig. 3(b), we obtain $T_2^* = 240$ ps (red line, $\exp(-t/T_2^*)$) for this particular SiV, in good agreement with previously measured values [24]. This is much shorter than the excited state lifetime of 1.7 ns at liquid helium temperature [10], and can be attributed to the fast decay into the lower excited state as well as any local strain in the material [28]. The strain may induce a phase shift and amplitude decrease in the averaged Ramsey interference fringes by distorting the lattice and breaking the inversion symmetry, which makes the color center more sensitive to the local electric field, and causes an emitter frequency shift with respect to the excitation laser frequency. In addition, the timescale of T_2^* is much larger than the pulse duration, which ensures minimal impact of the pulse shape on the measured T_2^* and visibility.

To demonstrate universal single qubit gate operation, we performed a complete coherent control, which allows for access to the entire Bloch sphere. Full SU(2) control of our qubit is achieved through a slight variation of the Ramsey interference experiment by driving the qubit with dual resonant pulses with both a variable area and a variable delay. As with the Ramsey experiments, we performed the SU(2) control at 66.7 ps coarse delay to avoid interference between the two pulses. After setting the amplitude of both pulses, the fine interpulse delay is scanned over 10 fs while recording the photon counts from the detection channel. The Ramsey-type interference experiment is repeated for all accessible pulse powers, and the resulting photon count map as a function of interpulse fine delay and individual pulse power is provided in Fig. 4(a), showing the typical multi-lobed structure expected of complete coherent control of resonantly driven qubits [1]. Quantum optics simulation of the SU(2) coherent control using parameters extracted from the Rabi oscillation and Ramsey interference is shown in Fig. 4(b). The phase shift at higher pulse powers in the experimental data is likely due to the residual spectral drift of the emitter during the several hours of acquisition time for the SU(2) control experiment.

4. CONCLUSION

We have demonstrated an on-chip platform based on arrays of diamond nanopillars with an ~150 nm device footprint featuring embedded individually addressable single SiV centers with a 31.3% yield. Using this platform, we have demonstrated full SU(2) coherent control of individual SiV centers using ultrafast optical pulses, which enables universal single qubit gate operation. Moreover, the coherent control of a SiV center inside a nanopillar structure is possible as a result of the high spectral stability of these SiV centers, despite the less than 75 nm distance from the diamond–air interface. Our demonstration paves the way for future integration of shallow SiV centers into nanophotonic devices for cavity quantum electrodynamics (QED) and spin-photon interfaces [29,30]. Thanks to the low inhomogeneous broadening compared to other solid-state platforms such as SiV in nanodiamonds or semiconductor quantum dots, it is therefore possible to envision entanglement of two low-strain single SiV centers hosted in different nanopillars. Finally, the ultrafast all-optical coherent control techniques demonstrated in this work can be extended to control the Zeeman-split spin states of SiV centers. The relatively short electron spin coherence time limited by the single phonon decoherence mechanism can potentially be alleviated in these small nanopillars due to the reduced phonon density of states. In conclusion, we believe we have shown a promising step toward a platform for scalable, on-chip quantum systems that could play an important role in future quantum hardware [31].

Funding. U.S. Department of Energy (DOE), Laboratory Directed Research and Development program at SLAC National Accelerator Laboratory (DE-AC02-76SF00515); Army Research Office (ARO) (W911NF1310309); Air Force Office of Scientific Research (AFOSR) through Multidisciplinary University Research Initiative (MURI) on Quantum Metaphotonics & Metamaterials (FA9550-12-1-0488); National Science Foundation (NSF) (ECS-9731293); Stanford Nano Shared Facility.

Acknowledgment. Jingyuan Linda Zhang acknowledges support from the Stanford Graduate Fellowship. Constantin Dory acknowledges support from the Andreas Bechtolsheim Stanford Graduate Fellowship.

†These authors contributed equally to this work.

See Supplement 1 for supporting content.

REFERENCES

1. K. G. Lagoudakis, P. L. McMahon, C. Dory, K. A. Fischer, K. Müller, V. Borish, D. Dalacu, P. J. Poole, M. E. Reimer, V. Zwiller, Y. Yamamoto, and J. Vučković, "Ultrafast coherent manipulation of trions in site-controlled nanowire quantum dots," Optica **3**, 1430–1435 (2016).
2. K. G. Lagoudakis, P. L. McMahon, K. A. Fischer, S. Puri, K. Müller, D. Dan, P. J. Poole, M. E. Reimer, V. Zwiller, Y. Yamamoto, and J. Vučković, "Initialization of a spin qubit in a site-controlled nanowire quantum dot," New J. Phys. **18**, 053024 (2016).
3. S. Unsleber, S. Maier, D. P. S. McCutcheon, Y.-M. He, M. Dambach, M. Gschrey, N. Gregersen, J. Mørk, S. Reitzenstein, S. Höfling, C. Schneider, and M. Kamp, "Observation of resonance fluorescence and the Mollow triplet from a coherently driven site-controlled quantum dot," Optica **2**, 1072–1077 (2015).
4. G. Balasubramanian, P. Neumann, D. Twitchen, M. Markham, R. Kolesov, N. Mizuochi, J. Isoya, J. Achard, J. Beck, J. Tissler, V. Jacques, P. R. Hemmer, F. Jelezko, and J. Wrachtrup, "Ultralong spin coherence time in isotopically engineered diamond," Nat. Mater. **8**, 383–387 (2009).
5. D. de Lange, Z. H. Wang, D. Riste, V. V. Dobrovitski, and R. Hanson, "Universal dynamical decoupling of a single solid-state spin from a spin bath," Science **330**, 60–63 (2010).
6. P. C. Maurer, G. Kucsko, C. Latta, L. Jiang, N. Y. Yao, S. D. Bennett, F. Pastawski, D. Hunger, N. Chisholm, M. Markham, D. J. Twitchen, J. I. Cirac, and M. D. Lukin, "Room-temperature quantum bit memory exceeding one second," Science **336**, 1283–1286 (2012).
7. Y.-C. Chen, P. S. Salter, S. Knauer, L. Weng, A. C. Frangeskou, C. J. Stephen, S. N. Ishmael, P. R. Dolan, S. Johnson, B. L. Green, G. W. Morley, M. E. Newton, J. G. Rarity, M. J. Booth, and J. M. Smith, "Laser writing of coherent colour centres in diamond," Nat. Photonics **11**, 77–80 (2017).
8. D. M. Toyli, C. D. Weis, G. D. Fuchs, T. Schenkel, and D. D. Awschalom, "Chip-scale nanofabrication of single spins and spin arrays in diamond," Nano Lett. **10**, 3168–3172 (2010).
9. A. Sipahigil, K. D. Jahnke, L. J. Rogers, T. Teraji, J. Isoya, A. S. Zibrov, F. Jelezko, and M. D. Lukin, "Indistinguishable photons from separated silicon-vacancy centers in diamond," Phys. Rev. Lett. **113**, 113602 (2014).
10. L. J. Rogers, K. D. Jahnke, T. Teraji, L. Marseglia, C. Muller, B. Naydenov, H. Schauffert, C. Kranz, J. Isoya, L. P. McGuinness, and F. Jelezko, "Multiple intrinsically identical single-photon emitters in the solid state," Nat. Commun. **5**, 4739 (2014).
11. E. Neu, D. Steinmetz, J. Riedrich-Möller, S. Gsell, M. Fischer, M. Schreck, and C. Becher, "Single photon emission from silicon-vacancy colour centres in chemical vapour deposition nano-diamonds on iridium," New J. Phys. **13**, 025012 (2011).
12. R. E. Evans, A. Sipahigil, D. D. Sukachev, A. S. Zibrov, and M. D. Lukin, "Narrow-linewidth homogeneous optical emitters in diamond nanostructures via silicon ion implantation," Phys. Rev. Appl. **5**, 044010 (2016).
13. J. Riedrich-Moller, L. Kipfstuhl, C. Hepp, E. Neu, C. Pauly, F. Mucklich, A. Baur, M. Wandt, S. Wolff, M. Fischer, S. Gsell, M. Schreck, and C. Becher, "One- and two-dimensional photonic crystal microcavities in single crystal diamond," Nat. Nanotechnol. **7**, 69–74 (2012).
14. B. J. Hausmann, I. B. Bulu, P. B. Deotare, M. McCutcheon, V. Venkataraman, M. L. Markham, D. J. Twitchen, and M. Loncar, "Integrated high-quality factor optical resonators in diamond," Nano Lett. **13**, 1898–1902 (2013).
15. A. Faraon, C. Santori, Z. Huang, V. M. Acosta, and R. G. Beausoleil, "Coupling of nitrogen-vacancy centers to photonic crystal cavities in monocrystalline diamond," Phys. Rev. Lett. **109**, 033604 (2012).
16. A. Sipahigil, R. E. Evans, D. D. Sukachev, M. J. Burek, J. Borregaard, M. K. Bhaskar, C. T. Nguyen, J. L. Pacheco, H. A. Atikian, C. Meuwly, R. M. Camacho, F. Jelezko, E. Bielejec, H. Park, M. Lončar, and M. D. Lukin, "An integrated diamond nanophotonics platform for quantum optical networks," Science **354**, 847–850 (2016).
17. J. Riedrich-Moller, C. Arend, C. Pauly, F. Mucklich, M. Fischer, S. Gsell, M. Schreck, and C. Becher, "Deterministic coupling of a single silicon-vacancy color center to a photonic crystal cavity in diamond," Nano Lett. **14**, 5281–5287 (2014).
18. J. L. Zhang, H. Ishiwata, T. M. Babinec, M. Radulaski, K. Muller, K. G. Lagoudakis, C. Dory, J. Dahl, R. Edgington, V. Souliere, G. Ferro, A. A. Fokin, P. R. Schreiner, Z. X. Shen, N. A. Melosh, and J. Vuckovic, "Hybrid group IV nanophotonic structures incorporating diamond silicon-vacancy color centers," Nano Lett. **16**, 212–217 (2016).
19. M. Radulaski, Y.-K. Tzeng, J. L. Zhang, K. G. Lagoudakis, H. Ishiwata, C. Dory, K. A. Fischer, Y. A. Kelaita, S. Sun, P. C. Maurer, K. Alassaad, G. Ferro, Z.-X. Shen, N. Melosh, S. Chu, and J. Vučković, "Diamond color center integration with a silicon carbide photonics platform," arXiv: 1610.03183 (2017).
20. T. Schröder, M. E. Trusheim, M. Walsh, L. Li, J. Zheng, M. Schukraft, R. M. Camacho, J. L. Pacheco, E. S. Bielejec, A. Sipahigil, R. E. Evans, D. D. Sukachev, C. T. Nguyen, M. D. Lukin, and D. Englund, "Scalable focused ion beam creation of nearly lifetime-limited single quantum emitters in diamond nanostructures," Nat. Commun. **8**, 15376 (2017).
21. L. J. Rogers, K. D. Jahnke, M. H. Metsch, A. Sipahigil, J. M. Binder, T. Teraji, H. Sumiya, J. Isoya, M. D. Lukin, P. Hemmer, and F. Jelezko, "All-optical initialization, readout, and coherent preparation of single silicon-vacancy spins in diamond," Phys. Rev. Lett. **113**, 263602 (2014).
22. B. Pingault, J. N. Becker, C. H. Schulte, C. Arend, C. Hepp, T. Godde, A. I. Tartakovskii, M. Markham, C. Becher, and M. Atature, "All-optical formation of coherent dark states of silicon-vacancy spins in diamond," Phys. Rev. Lett. **113**, 263601 (2014).
23. Y. Zhou, A. Rasmita, K. Li, Q. Xiong, I. Aharonovich, and W. B. Gao, "Coherent control of a strongly driven silicon vacancy optical transition in diamond," Nat. Commun. **8**, 14451 (2017).
24. J. N. Becker, J. Gorlitz, C. Arend, M. Markham, and C. Becher, "Ultrafast all-optical coherent control of single silicon vacancy colour centres in diamond," Nat. Commun. **7**, 13512 (2016).
25. B. Pingault, D. D. Jarausch, C. Hepp, L. Klintberg, J. N. Becker, M. Markham, C. Becher, and M. Atature, "Coherent control of the silicon-vacancy spin in diamond," Nat. Commun. **8**, 15579 (2017).
26. E. D. Kim, K. Truex, X. Xu, B. Sun, D. G. Steel, A. S. Bracker, D. Gammon, and L. J. Sham, "Fast spin rotations by optically controlled geometric phases in a charge-tunable InAs quantum dot," Phys. Rev. Lett. **104**, 167401 (2010).
27. K. D. Jahnke, A. Sipahigil, J. M. Binder, M. W. Doherty, M. Metsch, L. J. Rogers, N. B. Manson, M. D. Lukin, and F. Jelezko, "Electron-phonon processes of the silicon-vacancy centre in diamond," New J. Phys. **17**, 043011 (2015).
28. C. Arend, J. N. Becker, H. Sternschulte, D. Steinmüller-Nethl, and C. Becher, "Photoluminescence excitation and spectral hole burning spectroscopy of silicon vacancy centers in diamond," Phys. Rev. B **94**, 045203 (2016).
29. M. J. Burek, N. P. de Leon, B. J. Shields, B. J. Hausmann, Y. Chu, Q. Quan, A. S. Zibrov, H. Park, M. D. Lukin, and M. Loncar, "Free-standing mechanical and photonic nanostructures in single-crystal diamond," Nano Lett. **12**, 6084–6089 (2012).
30. M. J. Burek, D. Ramos, P. Patel, I. W. Frank, and M. Lončar, "Nanomechanical resonant structures in single-crystal diamond," Appl. Phys. Lett. **103**, 131904 (2013).
31. H. J. Kimble, "The quantum internet," Nature **453**, 1023–1030 (2008).